Remote Sens. **2015**, *7*, 8683-8704; doi:10.3390/rs70708683

OPEN ACCESS

remote sensing

ISSN 2072-4292

www.mdpi.com/journal/remotesensing

Article

Remote Sensing Observation of Particulate Organic Carbon in the Pearl River Estuary

Dong Liu [1,2], Delu Pan [1,2,*], Yan Bai [2], Xianqiang He [2], Difeng Wang [2], Ji-An Wei [2] and Lin Zhang [2]

[1] Department of Earth System, Zhejiang University, Hangzhou 310027, China; E-Mail: liudong6418sc@sina.com

[2] State Key Laboratory of Satellite Ocean Environment Dynamics, Second Institute of Oceanography, State Oceanic Administration, Hangzhou 310012, China; E-Mails: baiyan_ocean@126.com (Y.B.); hexianqiang@sio.org.cn (X.H.); dfwang@sio.org.cn (D.W.); anserwei@163.com (J.-A.W.); zhanglin@sio.org.cn (L.Z.)

* Author to whom correspondence should be addressed; E-Mail: pandelu@sio.org.cn; Tel.: +86-0571-8196-3201; Fax: +86-0571-8196-3112.

Academic Editors: Deepak R. Mishra and Prasad S. Thenkabail

Received: 25 March 2015 / Accepted: 26 June 2015 / Published: 9 July 2015

Abstract: River estuaries are connectors of terrestrial and marine ecosystems. Riverine particulate organic carbon (POC) is discharged into oceans after a series of biogeochemical reactions in estuaries. Satellite monitoring of POC will improve our understanding of the carbon dynamics of these water bodies. Based on *in situ* data from four seasonal survey cruises, we developed an algorithm for estimating POC concentrations in the Pearl River Estuary (PRE). Reflectance ratios, Rrs(678)/Rrs(488) and Rrs(748)/Rrs(412), were set as inputs to calculate POC concentration in the PRE. The algorithm was then applied to MODIS/AQUA data to inverse POC concentrations in the PRE from 2002 to 2014. Additionally, sources, impact factors, and seasonal distributions of POC were also investigated. Phytoplankton contributed more to POC in off-shore waters than that in in-shore waters in autumn and spring, but showed the opposite pattern in winter. Under the influence of freshwater from the Pearl River, underwater topography, tides, winds, *etc.*, the seasonal POC concentrations along a specific section, vertical to water depth gradient, decreased in different seasons. These decreases could be described by exponential functions ($y = ae^{bx}$, $b < 0$). The distribution of POC concentrations in the PRE resulted from complex physical and biogeochemical processes, which can change spatially and seasonally.

Keywords: Pearl River Estuary; particulate organic carbon; remote sensing; highly turbid water; impact factor

1. Introduction

Carbon is found widely in aquatic ecosystems in the form of dissolved organic carbon (DOC), particulate organic carbon (POC), dissolved inorganic carbon (DIC), and particulate inorganic carbon (PIC). In the ocean's euphotic layer, DIC together with nutrients can be used to produce POC through phytoplankton photosynthesis [1]. Oceanic POC includes biologically derived debris and autotrophic and heterotrophic microorganisms [1,2]. Although POC generally represents only around 4–5 × 10^9 t C of total carbon in marine surface waters, it plays an important role in the global carbon cycle [2]. POC is important in regards to its role in sequestering carbon, scavenging associated elements and compounds, and sinking to the bottom as part of "the biological pump" [1–3]. Moreover, compared with POC stock in the ocean surface, the flux from DIC to POC has been estimated at about 50 × 10^9 t C·yr^{-1} [2]. POC pool variation can reflect substantial changes in the related carbon pools, carbon fluxes, *etc.*

The concentration of POC in surface waters is affected by biological production, transformation to other carbon pools, downward export, *etc.* [2,4,5]. Temporal and spatial variations in ocean POC concentrations make characterizing it based on data taken from ships or other *in situ* measurements alone difficult [5]. Other technical means are needed. Suspended particles can scatter light back to space, with backscattered light being able to be received by remote sensing sensors. Some researchers have reported on relationships between POC concentration and particle backscattering light [5–7], and it has been suggested that POC concentrations in oceanic surface waters can be estimated from ocean color remote sensing data [2,3,5–8]. However, the spectral variability of the backscattering coefficients of suspended particles increases the difficulty in calculating POC from satellite data. At present, many remote sensing POC algorithms are based on the green band or green-to-blue ratio [3,5,9]; besides, many studies use the decreasing trend of b_b with wavelength [5,7,9]. In 1999, Stramski *et al.* [9] firstly published an algorithm for estimating POC concentration in the Southern Ocean from SeaWiFS data based on the correlation between the particle backscattering coefficient, $b_{bp}(\lambda)$, and POC concentration and the dependence of spectral reflectance, $R_{rs}(\lambda)$, on the total backscattering coefficient, $b_b(\lambda)$ [9]. Using *in situ* data from the eastern Atlantic Ocean [5] or field data from cruises across the Atlantic and Pacific [7], further algorithms were developed based on power function fitting between POC concentration and $R_{rs}(490)/R_{rs}(555)$ or $R_{rs}(443)/R_{rs}(555)$. Correlations between POC concentration and the diffuse attenuation coefficient at 490 nm, K_{490}, or the beam attenuation coefficient due to particles, C_p, were also used to estimate ocean POC concentration from satellite data [8]. All these algorithms were designed for retrieval of POC concentrations in open sea surface water or over the euphotic depth [10], where POC is mainly derived from phytoplankton and can even be estimated from Chl-*a* concentrations [5,11]. However, for waters along coastal zones, especially estuaries, POC is derived not only from phytoplankton but also from terrestrial ecosystems [12]. The variable particle assemblages (many mineral particles for example) and high concentrations of optically important dissolved organic matter (DOM) in coastal waters mean that open ocean POC algorithms do not perform well [3]. Although they

account for less than 10% of the world's ocean area, coastal oceans play an important role in the global carbon cycle. On the one hand, approximately 5×10^8 t of organic carbon from various terrestrial sources is transported into coastal waters by global rivers every year [13]; on the other hand, non-deltaic shelf deposits account for 45% of organic carbon burial in global oceans, which are thought to be the second largest sink of atmospheric CO_2 [14]. Son *et al.* [3] established the Maximum Normalized Difference Carbon Index (MNDCI) to estimate POC concentration in the Gulf of Mexico from remote sensing reflectance. However, the MNDCI does not perform well for highly turbid waters affected by rivers in the East Asian Monsoon region.

The Pearl River Estuary (PRE), which is covered by highly turbid waters, connects the Pearl River and the South China Sea. The POC in the PRE is sourced from both terrestrial and aquatic ecosystems. From November 2013 to August 2014, four seasonal survey cruises were undertaken to determine the sources and dynamics of POC in the PRE. Based on spectrum and POC data from the cruises, we first developed an estimation algorithm for surface POC concentrations in the highly turbid waters of the PRE. We then applied the algorithm to the MODIS/AQUA data to calculate seasonal POC in the PRE; sources, impact factors, and temporal and spatial variations of POC in the PRE were also examined.

2. Study Area

The PRE is located at 112.93°E–114.29°E and 21.31°N–22.86°N, ranging from the coastline of the Pearl River Delta to the northern South China Sea (Figure 1). The Pearl River Delta is one of the most prosperous regions in China. Intensive anthropogenic activities, including rapid industrialization and urbanization, have increased organic pollutant discharge into the PRE and eventually to open seas [15]. The northern part of Wanshan Archipelago (north of 22° N), also called Lingdingyang Bay, is severely affected by human activities due to a number of large Chinese metropolises are located in this area, including Hong Kong, Shenzhen, and Guangzhou, *etc.*

The PRE receives freshwater from the Pearl River via eight runoff outlets, which are all located along the western PRE coastline (Figure 1). The eastern side has two deep channels, along which saltwater can intrude into the HuMen outlet at high tide (Figure 1). A counter-clockwise current inside the PRE is present under these conditions [16]. The PRE is situated in the subtropical zone, and air temperature above the estuary does not change greatly. However, it is affected by the East Asian Monsoon by, for instance, receiving about 80% of its freshwater from nearby rivers during the wet season [15,17]. Ranked according to discharge, the Pearl River is the world's fourteenth largest and China's second largest river [18]. Every year, about 9.2×10^5 t of dissolved and particulate organic carbon, along with approximately 3.43×10^{12} m^3 freshwater from the Pearl River, are discharged into the PRE [15,18]. Among this, about 4.0×10^5 t is dissolved organic carbon (DOC) [15]. River water is a main source of chromophoric dissolved organic matter (CDOM) in the PRE, though co-variation between CDOM and DOC is absent [16].

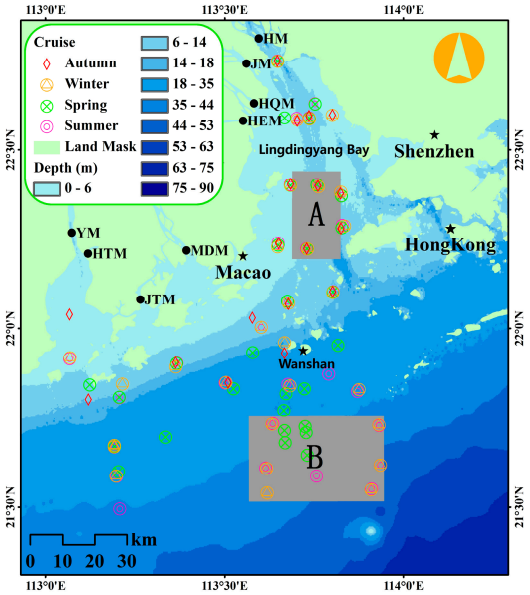

Figure 1. Schematic map of the Pearl River Estuary. Eight runoff outlets of the Pearl River are symbolized by black dots (●) and labeled as HM (HuMen), JM (JiaoMen), HQM (HongQiMen), HEM (HEngMen), MDM (MoDaoMen), JTM (JiTiMen), HTM (HuTiaoMen), YM (YaMen). The bathymetric chart was interpolated from water depth points of nautical charts in 2008, at the scale of 1:50,000. Region A and B were defined to discuss variations of annual mean POC concentration from 2002 to 2014, as discussed in Section 5.3.

3. Materials

3.1. Field Sampling and Laboratory Analyses

Four seasonal cruises were conducted from 18 to 22 November 2013 (autumn cruise), 26 February to 2 March 2014 (winter cruise), 10 to 14 May 2014 (spring cruise), and 24 to 30 August 2014 (summer cruise) (Figure 1). Using *Niskin* bottles, water samples were collected from 0.5 m below the water surface. The water samples were filtrated immediately through filters to assemble POC, chlorophyll a (Chl-*a*), and total suspended matter (TSM). Glass fiber filters (*Whatman*, 0.7 μm, and Φ47 mm) for POC samples had been pre-combusted at 450 °C for 5 h; after filtering, filters with POC were then packed in aluminum foils and stored in a refrigerator with a temperature around −20 °C. Chl-*a* samples were prepared by filtrating waters through glass fiber filters (*Whatman*, 0.7 μm, and Φ25 mm) without preprocessing; and filters with Chl-*a* were packed in aluminum foils and preserved in liquid nitrogen at a temperature around −200 °C. Each TSM sample was assembled by filtrating water through cellulose acetate membrane (*Satorius*, 0.45 μm, and Φ47 mm), which had been dried at 45 °C for 4 h repeatedly until the difference of weight between the pretreatment and post-treatment was less than 0.1 mg. The filters with TSM were then placed in culture dishes and stored in a refrigerator at −20 °C. The collection of samples followed the protocols of the Joint Global Ocean Flux Study (JGOFS) [19]; more details about Chl-*a* sampling could also refer to Liu *et al.* [20].

After returning to the laboratory, the POC samples were measured via the high temperature combustion method (680 °C) using a Total Organic Analyzer (*Shimadzu Incorporation*) [13]. Chl-*a* samples were measured using a Turner Designs Trilogy^{TM} Fluorometer. Each TSM sample was dried in

an oven at 40 °C for 6–8 h repeatedly until the difference of weight between the pretreatment and post-treatment was less than 0.1 mg; the TSM weight was then calculated through the quality difference method [21]. Details on Chl-*a* measurement can be found in Liu *et al.* [20].

3.2. Measurement of Remote Sensing Reflectance

Radiance spectra were measured using a FieldSpec Spectroradiometer (*Analytical Spectral Devices Incorporation*, *ASD*, *Boulder*, *CO*, *USA*) with a spectral range of 350 nm to 2390 nm and a resolution of 1 nm. We measured radiance of water (L_{ws}) and radiance of skylight (L_{sky}) with the probe positioned at an angle of 90°–135° to the plane of incident radiation in order to minimize the effects of sunlight and the ship's shadow. The view angle of the probe for L_{ws} was 30°–45° to the aplomb direction, but 135°–150° for L_{sky}. After measurements of L_{ws} and L_{sky}, radiance of the standard gray board (L_p) was measured as similar to L_{ws}. Because of poor sea conditions or occasional factors, spectra were not measured at every designed station. Spectral measurement followed the Ocean Optical Protocols proposed by NASA [21,22]. From L_{ws}, L_{sky}, and L_p, the remote sensing reflectance (R_{rs}) of water was computed using Equation (1).

$$\begin{cases} R_{rs} = L_w / E_s(0^+) \\ L_w = L_{ws} - r \cdot L_{sky} \\ E_s(0^+) = \pi \cdot L_p / \rho \end{cases} \quad (1)$$

where, L_w is the water-leaving radiance; $E_s(0^+)$ is the incident irradiance to the water; r is the reflectance of the air-water interface, r = 0.028 for mixing waters in the PRE; and ρ represents reflectance of the standard gray board, obtained from calibration processes. Figure 2 shows the reflectance spectra ranging from 350 nm to 800 nm, which contain commonly used ocean color bands. Reflectance spectra at stations with high POC concentrations presented absorption peaks around 670 nm and fluorescence peaks around 690 nm. Reflectance spectra of several stations with different POC concentrations measured in the summer cruise are shown in Figure 2.

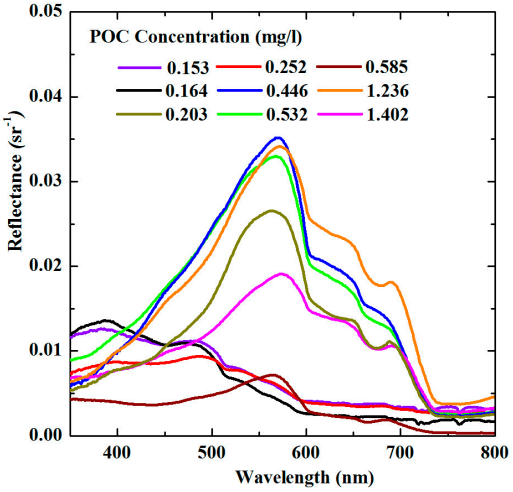

Figure 2. Reflectance spectra of water in the PRE. Water-leaving reflectance was calculated using Equation (1). Both water-leaving reflectance and POC concentration differed with stations.

3.3. Satellite Ocean Color Data

We also obtained daily Level 1B calibrated radiance products (MYD021KM, version 2.16) scanned by the Moderate Resolution Imaging Spectroradiometer (MODIS) onboard the AQUA satellite from the Level 1 and Atmosphere Archive and Distribution System (LAADS Web, http://ladsweb.nascom.nasa.gov/). The MODIS/AQUA data have a resolution of 1 km at ocean monitoring bands. All MODIS/AQUA data were observed at about 1:30 pm local time. The near-infrared and shortwave infrared bands (NIR-SWIR) atmospheric correction approach was applied to remove atmospheric effects and calculate water-leaving reflectance from MYD021KM [23]. The NIR-SWIR algorithm can derive water-leaving reflectance of open ocean turbid coastal waters at the same time [23].

4. Algorithm Development

To develop an algorithm for POC concentration estimation, we first calculated equivalent reflectance for eight ocean color bands of MODIS/AQUA data, with central wavelengths at 412 nm, 443 nm, 488 nm, 531 nm, 551 nm, 667 nm, 678 nm, and 748 nm respectively. For a specific band with a central wavelength at λ, equivalent reflectance was computed through Equation (2).

$$\begin{cases} r_{\text{equi}} = \dfrac{\int_{\lambda_{\min}}^{\lambda_{\max}} f(\lambda) r(\lambda) L(\lambda) d\lambda}{\int_{\lambda_{\min}}^{\lambda_{\max}} f(\lambda) L(\lambda) d\lambda} \end{cases} \tag{2}$$

where, $r_{\text{equi}}(\lambda)$ is the equivalent reflectance for a band with a central wavelength at λ; $f(\lambda)$ is the spectral response function, downloaded from OceanColor Website (http://oceancolor.gsfc.nasa.gov/); $r(\lambda)$ is the reflectance shown in Figure 2; $L(\lambda)$ is the solar irradiance at mean Earth-Sun distance; $\lambda_{\min}$ is equal to 350 nm, and 800 nm for $\lambda_{\max}$.

Both particulate and dissolved materials in water influence water-leaving reflectance. An algorithm using the reflectance ratio can decrease the effect of atmospheric correction [5]. Many ocean color algorithms have been developed using the reflectance ratio [5,7,21,24]. We design our algorithm for POC concentration in the PRE as Equation (3).

$$\begin{cases} \text{POC}_{\text{modeled}} = b_0 + b_1 \cdot Ratio_1 + b_2 \cdot Ratio_2 \\ Ratio_1 = r_{equi}(\lambda_1) / r_{equi}(\lambda_2) \\ Ratio_2 = r_{equi}(\lambda_3) / r_{equi}(\lambda_4) \end{cases} \tag{3}$$

where, $\text{POC}_{\text{modeled}}$ is the modeled POC concentration; *Ratio1* and *Ratio2* are the reflectance ratios of water-leaving reflectance; $r_{\text{equi}}(\lambda)$ is defined in Equation (2); and b_0, b_1, b_2 are constants.

In situ data collected in winter and summer cruises, 45 samples in all (red dots in Figure 3a), were used to train the algorithm. To determine the best band combination, correlation coefficient (R^2), Mean Square Error (RMSE), Absolute Error (AE), and Relative Error (RE) were employed to evaluate the result of each band combination. Definitions of AE and RE are as per Świrgoń *et al.* [25] and are defined in Equation (4).

$$\begin{aligned} \text{AE} &= \left| \text{POC}_{\text{modeled}} - \text{POC}_{\text{in-situ}} \right| \\ \text{RE} &= \left| \text{POC}_{\text{modeled}} - \text{POC}_{\text{in-situ}} \right| / \text{POC}_{\text{in-situ}} * 100\% \end{aligned} \tag{4}$$

where $POC_{in\text{-}situ}$ is the *in situ* POC concentration; $POC_{modeled}$ is the modeled POC concentration; and N is the total number of training data, $N = 45$.

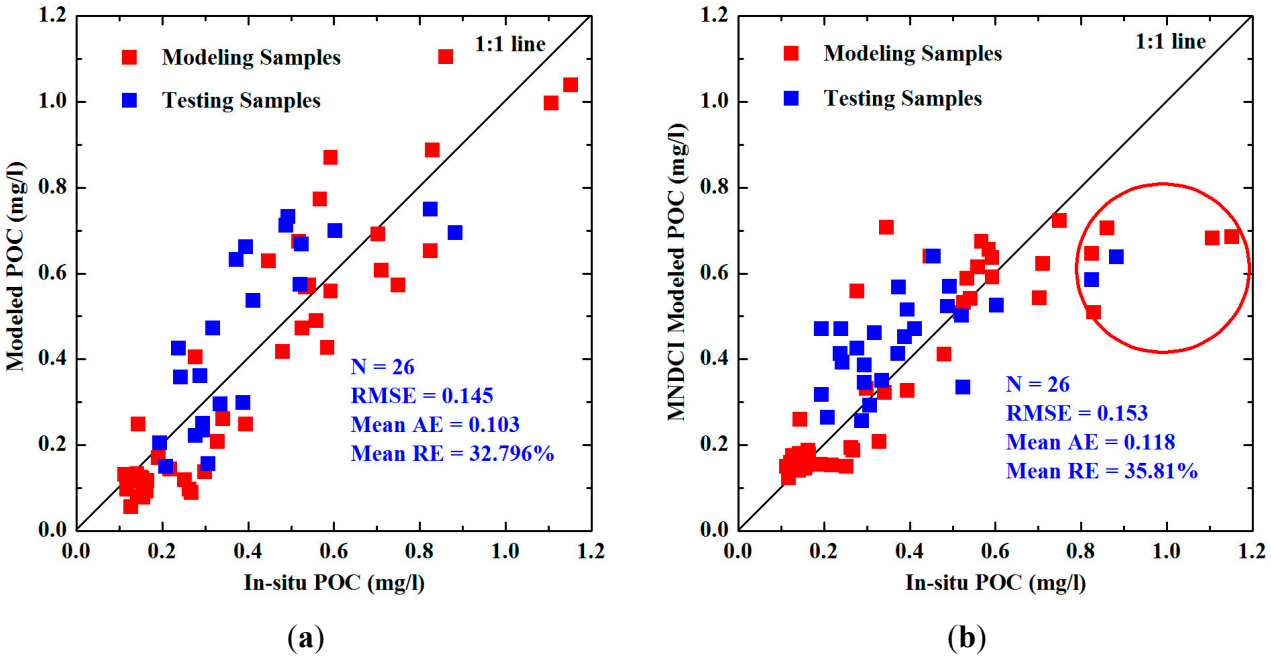

Figure 3. Comparisons between *in situ* POC and modeled POC concentrations using the algorithm developed in this study (**a**) and by Son *et al.* [3] (**b**). AE and RE are defined in Equation (4).

Based on Equation (3), band tuning and accuracy optimization [26,27] were used to find the optimal bands for λ_1, λ_2, λ_3, and λ_4, from the eight ocean color bands of MODIS/AQUA. After testing all possible band combinations, the algorithm achieved a best fitting result with $R^2 = 0.865$ and AE = 0.0932 mg/L when $\lambda_1 = 678$ nm, $\lambda_2 = 488$ nm, $\lambda_3 = 748$ nm, and $\lambda_4 = 412$ nm. We also obtained the regression coefficients for the algorithm, with $b_0 = 0.0078$, $b_1 = 1.3973$, and $b_2 = -1.2397$. In other words, surface POC concentrations in the PRE could be estimated through the following equation.

$$\begin{cases} POC_{modeled} = 0.0078 + 1.3973 \cdot Ratio_1 - 1.2397 \cdot Ratio_2 \\ Ratio_1 = r_{equi}(678) / r_{equi}(488) \\ Ratio_2 = r_{equi}(748) / r_{equi}(412) \end{cases} \quad (5)$$

All four bands are commonly used by ocean color researchers: 412 nm, where CDOM has a high absorption coefficient, is often used to inverse CDOM concentration [24]; 488 nm or 748 nm, where suspended particles have a high backscattering coefficient, are often used to inverse TSM concentration [21]; and 678 nm, containing a fluorescence signal from Chl-*a*, is often used to inverse Chl-*a* concentration [26,27].

5. Results

5.1. Application of the Developed Algorithm

5.1.1. Application to *in Situ* Data

Parameterized Equation (5) was applied to the *in situ* data collected in autumn and spring cruises, accounting for 26 samples (blue dots in Figure 3a). Figure 3a shows the comparison between *in situ* POC and modeled POC using the algorithm developed above. For all tested samples, the modeled POC concentrations were greater than the *in situ* values when *in situ* POC concentrations were higher than 0.4 mg/L and lower than 0.6 mg/L. Moreover, most modeled POC concentrations were lower than *in situ* POC concentrations for samples with low *in situ* POC concentrations (Figure 3a). However, results of applying the developed algorithm to *in situ* data were acceptable, with a mean AE of 0.103 mg/L and a mean RE of 32.796% for all tested samples.

By matching the *in situ* POC data with SeaWiFS reflectance, Son *et al.* [3] developed the MNDCI remote sensing algorithm to estimate water surface POC concentration in the northeastern Mexico Gulf, with almost all POC concentrations used for algorithm development lower than 0.7 mg/L. The MNDCI is shaped by Equation (6). In this paper, 45 samples from the winter and summer PRE cruises were used to compute the coefficients in Equation (6). The parameterized equation was then applied to 26 samples from the autumn and spring PRE cruises. Figure 3b shows the comparison between the *in situ* POC and modeled POC concentrations using the MNDCI. For all tested samples, most modeled POC concentrations were greater than the *in situ* values for samples with *in situ* POC concentrations lower than 0.5 mg/L. With a mean AE of 0.118 mg/L and mean RE of 35.81% for all tested samples, the overall estimation accuracy when applying the MNDCI to inverse the PRE POC concentrations was slightly lower than that of the algorithm developed in this paper (Figure 3). It would appear that the algorithm developed by Son *et al.* [3] was invalid for coastal waters where POC concentrations were greater than 0.8 mg/L. For PRE, all modeled POC concentrations using the MNDCI were lower than 0.7 mg/L when *in situ* values were higher than 0.8 mg/L (red circles in Figure 3b).

$$\begin{cases} \mathrm{POC} = 10^{b_5 MNDCI^5 + b_4 MNDCI^4 + b_3 MNDCI^3 + b_2 MNDCI^2 + b_1 MNDCI + b_0} \\ MDNDCI = \frac{r_{equi}(555) - max(r_{equi}(412), r_{equi}(443), r_{equi}(490))}{r_{equi}(555) + max(r_{equi}(412), r_{equi}(443), r_{equi}(490))} \end{cases} \quad (6)$$

where POC represents POC concentration, and $r_{equi}(412)$, $r_{equi}(443)$, $r_{equi}(490)$, and $r_{equi}(555)$ are defined in Equation (2).

5.1.2. Application to MODIS/AQUA Data

The new POC algorithm was developed by considering central wavelengths and spectral response functions of ocean color bands of MODIS/AQUA (Section 4). In this section, we applied the new algorithm to estimate POC concentrations in the PRE by inputting reflectance ratios of the MODIS/AQUA data from 2002 to 2014. Table 1 shows the comparisons between *in situ* POC concentrations and modeled POC concentrations using the newly developed algorithm. Modeled POC in Table 1 denotes the mean value of the 3 × 3 pixels window with central pixel covering the location of

in situ data. Due to cloud cover, only nine samples with *in situ* POC concentrations were found. The nine samples were sampled within four hours prior to or after the passing time of the AQUA satellite.

The mean AE of the modeled POC concentrations from the MODIS/AQUA data was 0.099 mg/L, with a minimum of 0.001 mg/L and maximum of 0.476 mg/L (Table 1), and the mean RE was 19.736%, with a minimum of 0.116% and maximum of 46.825%. When the difference between sampling time and passing time of MODIS/AQUA was large, such as No. 3 in Table 1, AE or RE was large. The RE of the modeled POC concentration was less than 35% for samples collected within three hours prior to or after the passing of the AQUA satellite. On the whole, the developed algorithm could be applied to estimate POC concentration in the PRE based on the MODIS/AQUA data. A good linear relationship was found between the *in situ* and modeled POC, with an R^2 of 0.855.

Table 1. Comparison results between *in situ* and modeled POC concentrations using the algorithm developed in this study. AE and RE are defined in Equation (4). Sampling time is the local time when MODIS/AQUA was passing.

No.	Sampling Day	Sampling Time	*In Situ* POC (mg/L)	Modeled POC (mg/L)	AE (mg/L)	RE (%)
1	27/2/2014	14:55	0.121	0.120	0.002	1.653
2	27/2/2014	14:04	0.150	0.117	0.033	22
3	27/2/2014	10:06	0.126	0.067	0.059	46.825
4	27/2/2014	11:15	0.113	0.077	0.036	31.858
5	24/8/2014	14:11	0.861	0.860	0.001	0.116
6	24/8/2014	9:24	1.402	0.926	0.476	33.952
7	24/8/2014	15:14	0.446	0.475	0.028	6.278
8	30/8/2014	12:00	0.829	0.755	0.074	8.926
9	30/8/2014	9:26	0.711	0.895	0.185	26.02

The Ocean Biology Processing Group (OBPG) recommends using Equation (7) as the standard algorithm to estimate global ocean surface POC concentration [7]. For the PRE, however, considerable differences were found in POC using option 2 and option 1 (Equation (7)). In addition, POC concentrations obtained using Equation (7) decreased when the POC concentrations in the PRE increased. In other words, the standard OBPG algorithm for POC estimation was not suitable for coastal waters in the PRE.

$$\begin{aligned} &\text{Option1:}\quad \mathrm{POC} = 203.2 \times \frac{r_{equi}(443)}{r_{equi}(555)}^{-1.034} \\ &\text{Option2:}\quad \mathrm{POC} = 308.3 \times \frac{r_{equi}(490)}{r_{equi}(555)}^{-1.639} \end{aligned} \tag{7}$$

where, POC represents POC concentration, and $r_{\mathrm{equi}}(443)$, $r_{\mathrm{equi}}(490)$, and $r_{\mathrm{equi}}(555)$ are defined in Equation (2).

5.2. Particulate Organic Carbon (POC) Distribution from in situ *Data*

For all 103 samples collected during the four seasonal cruises, the POC concentration ranged from 0.113 mg/L to 1.402 mg/L, with a minimum of 0.113 mg/L in winter and a maximum of 1.402 mg/L in

summer (Table 2). *In situ* data showed there was a wide range of POC concentrations in the PRE (Table 2). All designed stations were covered in the winter and summer cruises (Figure 1). Average POC concentration in the winter cruise was 0.393 mg/L, and in the summer cruise was 0.592 mg/L. Generally, the POC concentration in summer was greater than that from the other three seasonal cruises, especially for stations with salinity lower than 28 PSU (Figure 4).

Table 2. Descriptive statistics of *in situ* POC concentrations (mg/L) in the PRE. Due to rough sea conditions, not all designed stations were covered, especially those located south of 22° N in the autumn and spring cruises (Figure 1).

Cruise	Samples	Min	Max	Median	Mean
Autumn	18	0.156	1.150	0.260	0.348
Winter	27	0.113	1.374	0.277	0.393
Spring	29	0.194	0.883	0.372	0.420
Summer	29	0.118	1.402	0.557	0.592
All	103	0.113	1.402	0.349	0.449

For each cruise, the POC concentrations at different stations varied considerably (Table 2). Figure 4 shows the differences at different stations over the four seasonal cruises. The POC concentrations at stations where salinities were lower than 33 PSU changed more drastically. These stations were closer to the shore and were more affected by freshwater from the Pearl River. However, POC concentrations at stations where salinities were higher than 33 PSU (red circles in Figure 4) were around 0.2 mg/L. However, no clear negative relationship between POC concentration and salinity was observed.

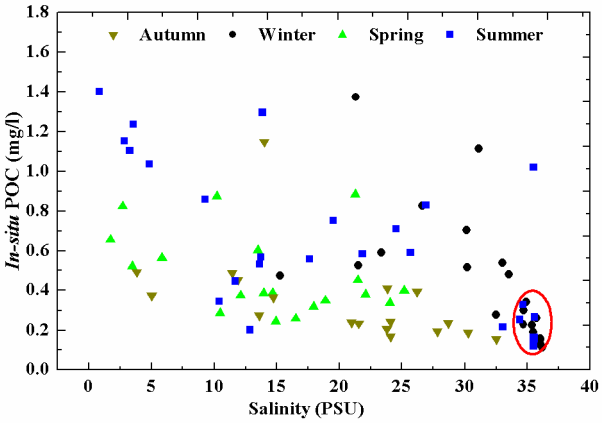

Figure 4. Changes in POC concentrations with salinity (Practical Salinity Units, PSU) in different cruises. Salinity was recorded by a multi-parameter water quality monitor (SBE 19Plus, Sea-Bird Electronics, Inc.: Bellevue, WA, USA).

5.3. Temporal and Spatial Variations from Satellite-Derived POC

By applying the developed algorithm to the reflectance ratios of MODIS/AQUA, we obtained the distribution of POC concentration in the PRE. We then computed seasonal POC concentration by averaging all daily POC values in four designated months from 2002 to 2014, which included 20 values in January for winter, 16 in April for spring, 24 in July for summer, and 34 in November for

autumn. Figure 5 shows the seasonal POC concentrations in the four specific months. Seasonal POC results were used to analyze the seasonality of POC distribution. In Lingdingyang Bay, POC concentrations were higher in the west than those in the east, especially in spring and autumn; however, this distribution pattern was not obvious in summer. In the southern Wanshan Archipelago, POC concentration decreased from the northwest to the southeast, with higher values in near-shore waters; moreover, the area where POC concentrations were larger than 0.3 mg/L was larger in summer than those in the other three seasons.

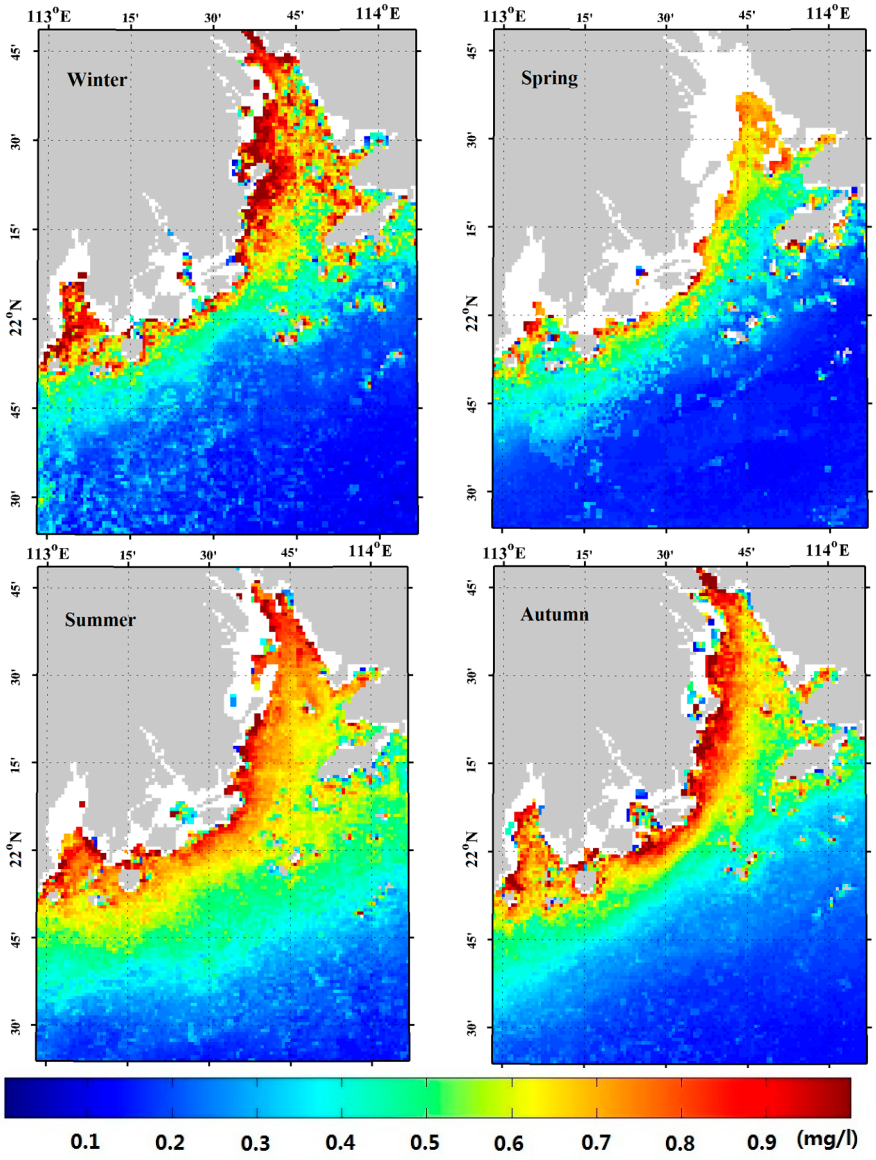

Figure 5. Seasonal POC concentrations (mg/L) derived from the MODIS/AQUA data from 2002 to 2014 using the proposed algorithm. Each season is represented by a specific month: January for winter, April for spring, July for summer, and November for autumn. The white regions are covered by highly turbid waters. Radiance of these regions was beyond the maximum radiance that band 13 or 14 of MODIS/AQUA can record, that is, band saturation occurred. Because of this, we did not obtain valid POC concentrations in the white regions. The pink line shows the vertical to water depth gradient section used to describe spatial variations of POC in the PRE.

To better understand POC distribution in the PRE, we defined a section (pink line in Figure 5) to quantitatively describe temporal and spatial variations of POC concentration in the PRE. This section starts in Lingdingyang Bay (113.61° E, 22.36° N) and ends in southeast of the study area (114.12° E, 21.39° N). The section was perpendicular to the isoline of water depth (Figures 1 and 6). POC concentrations along the section are shown in Figure 6. For all seasons, POC concentrations decreased along the section. POC concentrations decreased more remarkably in northern Wanshan at longitudes smaller than 113.8° E. The decreasing trends observed in all seasons can be described using exponential functions ($y = ae^{bx}$, $b < 0$), with $R^2 = 0.94$ for winter, $R^2 = 0.75$ for spring, $R^2 = 0.96$ for summer, and $R^2 = 0.96$ for autumn. It is worth noting there were POC concentration peaks around the Wanshan Archipelago (~113.8° E) in all seasons except summer.

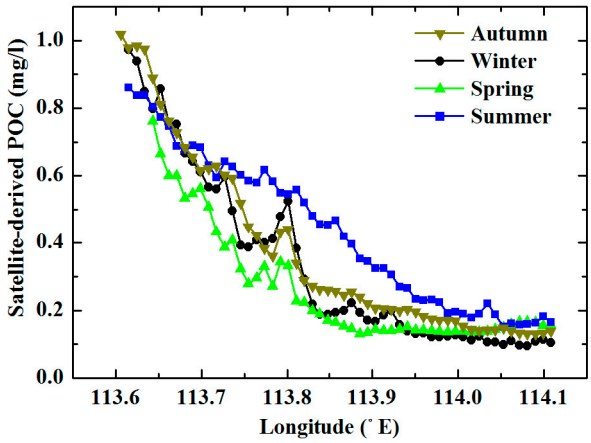

Figure 6. Seasonal POC concentrations (mg/L) along the section defined in Figure 5. The Wanshan Archipelago is located around 113.8° E. Each season is presented by a specific month: January for winter, April for spring, July for summer, and November for autumn.

Two regions were also defined in this study to present annual variations in PRE POC concentrations from 2002 to 2014. Region A was located in the Lingdingyang Bay, which was affected obviously by freshwater; and region B was located in the southern Wanshan Archipelago (Figure 1). Annual POC concentrations were calculated by averaging all satellite-derived daily POC values in region A or region B in January, April, July, and November of each year. Annual POC concentrations in region A were much greater than those in region B (Figure 7a). Mean annual POC concentration from 2002 to 2014 was 0.614 mg/L in region A and 0.182 mg/L in region B. Annual POC concentrations from 2002 to 2014 in region A fluctuated significantly around 0.614 mg/L, with a minimum of 0.474 mg/L in 2006 and maximum of 0.742 mg/L in 2009. The standard deviation of annual POC concentration in region A from 2002 to 2014 was 0.077 mg/L. There was a negative relationship between annual POC concentration in region A and discharge from the Pearl River (Figure 7b). Excluding data from 2011 with the lowest discharge and 2008 with the largest discharge, the significant negative correlation can be expressed by a linear Equation (Figure 7b). However, annual POC concentrations from 2002 to 2014 in region B did not change obviously, with a minimum of 0.168 mg/L in 2005 and maximum of 0.199 mg/L in 2009. The standard deviation of annual POC concentration in region B from 2002 to 2014 was 0.009 mg/L. Figure 7b also shows that POC concentration in PRE off-shore water was little affected by discharge

from the Pearl River. Moreover, the linear relationships between time and annual POC in region A (R^2 = 0.0103, significance level P = 0.7419 > 0.05) and region B (R^2 = 0.1986, significance level P = 0.1269 > 0.05) show that annual POC in the PRE did not increase or decrease from 2002 to 2014.

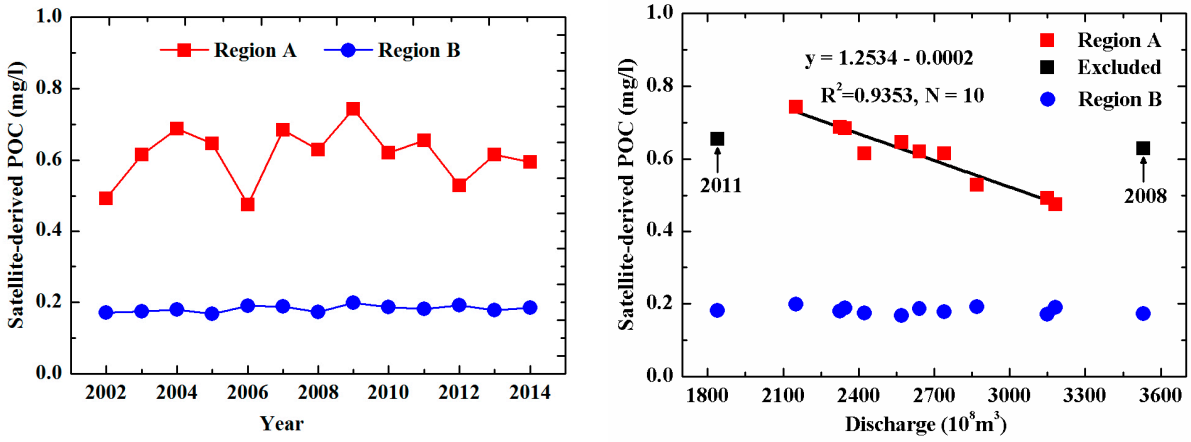

Figure 7. Annual satellite-derived POC in the PRE in different years: (**a**) Annual POC concentrations in region A and B, which are defined in Figure 1; (**b**) relationship between annual POC in the PRE and discharge of the Pearl River. Pearl River discharge was calculated from the daily discharge of three control hydrometric stations, Boluo, Shijiao, and Gaoyao.

6. Discussions

6.1. Sources of POC in the Pearl River Estuary

On a global scale, approximately 200 Tg (Tg = 1 × 10^{12} g) of terrestrial POC is poured into marginal oceans by rivers annually [13]. POC is one component of TSM, with POC(%TSM) denoting the percentage of POC in TSM [28,29]. Previous studies have described negative relationships between POC(%TSM) and TSM concentrations in numerous river systems [30–32]. We collected POC and TSM data from the world's major rivers and developed a power function ($y = 16.191x^{-0.395}$, R^2 = 0.602) to describe the correlation between POC(%TSM) and TSM concentration, which showed that the POC(%TSM) in different rivers differed from each other (Figure 8a). Monsoon rivers, such as the Ganges River, Changjiang River, and Mekong River, were characterized by high POC concentrations but low POC(%TSM). Conversely, non-monsoon rivers, such as the St. Lawrence River, Congo River, and Amurm River, were characterized by low POC concentrations but high POC(%TSM) (Figure 8a). Precipitation and river discharge from monsoon regions occur mainly in the wet season [17,33]. High intensity rainfall over monsoon regions in the wet season can lead to severe terrestrial erosion, resulting in an increase in TSM in rivers. When the TSM concentration is high, primary production of phytoplankton can decrease due to light limitation [34]. Thus, allochthonous POC becomes the major source of POC, and POC(%TSM) will decrease. This situation shows the opposite pattern in non-monsoon rivers. Of course, basin characteristics might also influence POC(%TSM), such as what observed in the Nile River and Yellow River (not included). Based on our four seasonal cruises, Figure 8b shows the relationship between POC(%TSM) and TSM concentration in the PRE, as also described

through the power function ($y = 21.630x^{-0.637}$, $R^2 = 0.756$). The PRE receives freshwater from the Pearl River. However, the POC(%TSM) in the PRE differed from that in the Pearl River. POC(%TSM) in the PRE ranged from 1.262% to 50.377%, with an average of 11.111%, while annual POC(%TSM) in the Pearl River was only 2% (Figure 8). This considerable difference might be due to additional POC sourced from phytoplankton in the more clear waters of PRE [12].

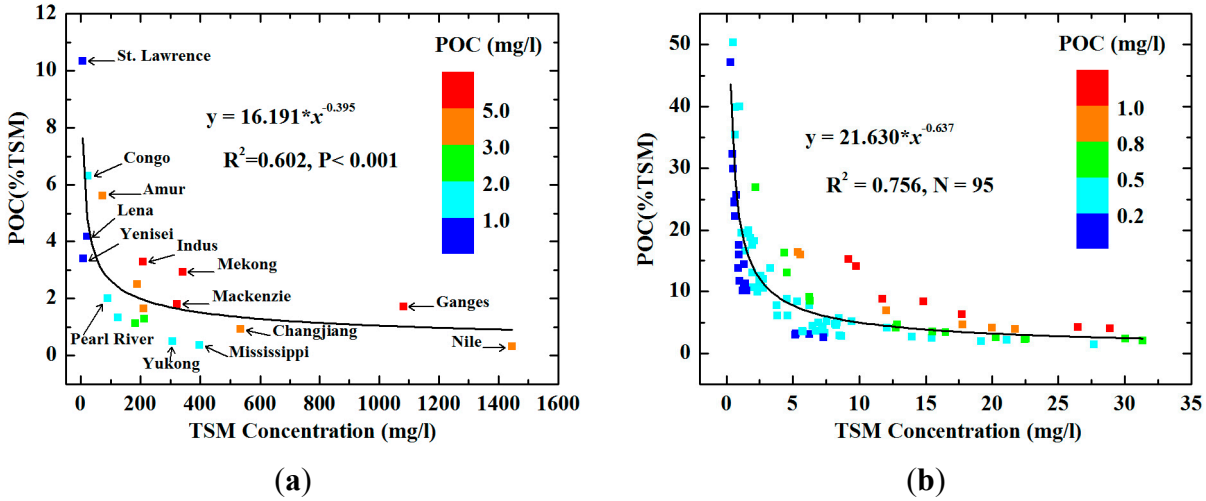

Figure 8. Correlation between POC(%TSM) and TSM concentration in: (**a**) 19 of the world's major rivers (from Dagg *et al.* [35], Ni *et al.* [15], Ran *et al.* [33], and Coynel *et al.* [34]); and (**b**) the Pearl River Estuary (from our four seasonal cruises).

Estuaries are the mixing zone between freshwater and seawater, and thus sources of POC in estuaries are complicated. Terrestrial POC comes from terrestrial ecosystems and is produced primarily through photosynthesis of vegetation, while aquatic POC comes from aquatic ecosystems and is produced primarily through photosynthesis of phytoplankton [12,36,37]. Many methods have been used to explore sources of POC in estuaries, including the elemental ratio of carbon to nitrogen (C/N), stable isotope composition ($\delta^{13}C$), and stable isotope signature of particulate nitrogen ($\delta^{15}N$), *etc.* [38]. Phytoplankton contributed significantly to POC in the PRE. The positive correlation between Chl-*a* and POC concentration was fitted through exponential function, with $R^2 = 0.541$ and $p < 0.001$ (Figure 9a). In accordance with Ni *et al.* [15], we also found a positive correlation between TSM and POC concentration in the PRE (Figure 9b). Around the outlets of HongQiMen and HEngMen, Liu *et al.* [12] reported that waters had high TSM and low Chl-*a* concentration. Therefore, POC concentrations in these waters appear to be majorly affected by POC transported by the Pearl River from land. Using $\delta^{13}C$, Liu *et al.* [12] also investigated the mixed terrestrial and aquatic sources of POC in the PRE and found that in summer, POC in the north and middle region was primarily sourced from terrestrial ecosystems (64%), but POC in the southern region was mainly from aquatic ecosystems (68%) [12].

Although the POC/Chl-*a* ratio might vary over a broad range in different ocean areas, POC/Chl-*a* can be used to explore sources of POC [39]. The influence of Chl-*a* on POC shows a constant value when data are constrained to regions with less terrestrial input [5]. Stramska *et al.* [5] estimated the POC concentration from Chl-*a* in the North Polar Atlantic based on a linear equation. Similar to open seas,

the POC concentrations in off-shore areas of the PRE, where waters were deeper than 18 m, were little affected by freshwater from the Pearl River, especially in seasons with small discharge [16]. There was a strong linear relationship between Chl-*a* and POC concentration in these waters (Figure 10). According to Eppley *et al.* [39], the linear regression slope of POC on Chl-*a* by weight provides information on the carbon/Chl-*a* ratio of phytoplankton, while the intercept provides the non-algal POC. POC concentrations in off-shore areas of the PRE can also be estimated from Chl-*a*. As seen in Figure 10, phytoplankton with 1 μg of Chl-*a* contained about 0.129 mg of POC in off-shore waters. Based on this, POC = 0.231 mg/L at Chl-*a* = 1 μg/L in off-shore waters. For regional PRE, we first assumed that phytoplankton communities were similar. We then estimated the phytoplankton contribution to POC in the PRE from the Chl-*a* data collected from the seasonal cruises (Table 3). In autumn and spring, phytoplankton contributed more to POC in off-shore waters than that in in-shore waters; however, phytoplankton contributed more to POC in in-shore waters than that in off-shore waters in winter. This phenomenon was likely the result of smaller riverine POC flux, together with smaller discharge, from the Pearl River in winter [15,17]. We assumed that phytoplankton communities were similar in regional PRE so as to calculate the contribution of phytoplankton to POC semi-quantitatively. However, spatial variability of the phytoplankton community structure might exert an effect on POC/Chl-*a* variations. Based on only one cruise in April 2007, He *et al.* [40] also reported that POC and Chl-*a* had a significant positive correlation in the freshwater region of the PRE (including part of the Pearl River), with the POC/Chl-*a* regression slope being only 0.0234 by weight. Therefore, the contribution of phytoplankton to POC in in-shore waters might have been overestimated.

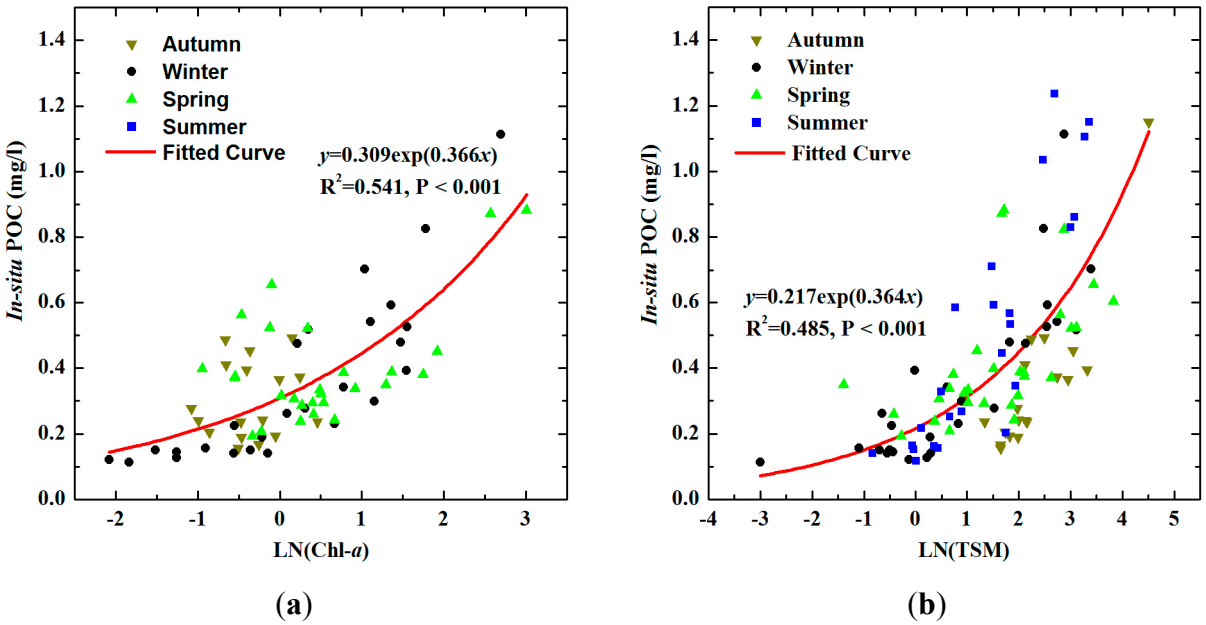

Figure 9. Relationship between POC concentration in the PRE and ocean color parameters: (**a**) Chl-*a*; (**b**) TSM. Chl-*a* data are not available for the summer cruise.

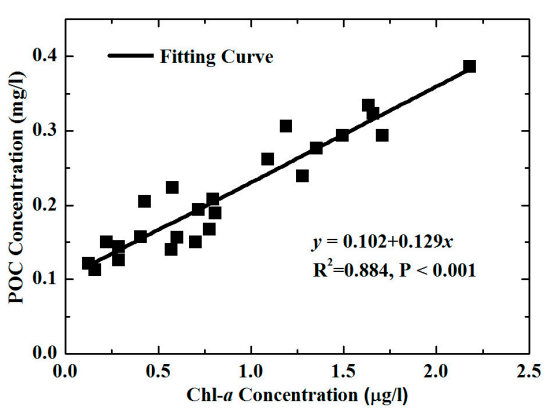

Figure 10. Correlation between POC concentrations and Chl-*a* concentrations for stations located in off-shore areas, where waters were deeper than 18 m (Figure 1). Summer data are not included.

Table 3. Contribution of phytoplankton to POC in different seasons and water types. Chl-*a* data was not available for the summer cruise. Off-shore waters contained stations with waters deeper than 18 m.

Season	Phytoplankton POC (%)	
	In-shore Waters	Off-shore Waters
Autumn	33.26	45.3
Winter	62.5	40.59
Spring	29.16	65.32

6.2. Impact Factors on POC Distribution in the PRE

After entering marginal oceans, riverine POC will experience a series of biogeochemical reactions. Part of riverine POC will be decomposed by bacteria, zooplanktons, viruses, *etc.*, [35,41]. In addition, different sized POC will be partitioned in estuaries and further partitioned when transported along-shore or across-shelf [14]. Large POC particles are prone to settle down to the seafloor; however, tiny POC particles might be transported to the continental shelf, or even open seas, by currents [32]. Except for riverine POC, salinity-induced flocculation of dissolved organic carbon (DOC) to POC might increase POC concentration in coastal oceans [41]. Moreover, phytoplankton production in some parts of the river plume will be generally high because of rich available nutrients, buoyant freshwater, and adequate light penetration [35]. However, the location of maximum phytoplankton production along the salinity gradient might change with seasons and estuary conditions [35]. Of course, benthic resuspension, which occurs primarily in winter in the PRE, can also increase POC concentrations in coastal waters [1,12]. Thus, the distribution of POC in coastal oceans is strongly influenced by all these major processes.

Seawater can intrude into the PRE from the east, while most freshwater from the Pearl River is discharged into the western PRE. Water masses mixing processes can influence the spatial distribution of POC concentration in the PRE. Seawater with lower POC concentrations can prevent freshwater from spreading to the east (Figure 5). Like in many other estuaries, freshwater, usually with higher POC concentrations, will be diluted by seawater [1,3,42]. Therefore, POC concentrations in the west were

generally greater than those in the east (Figure 5). In the PRE, POC concentration decreased with distance from the Pearl River outlets (Figures 5 and 6). *In situ* data in the different seasons also showed that POC concentrations decreased with increasing salinity (Figure 4). Based on more than 10 years of data, the exponential function ($y = ae^{bx}$, $b < 0$) also described the decrease in seasonal POC with increasing distance from the coastline (Figure 6). Along the specific section (Figure 5), seasonal POC in different seasons were approximate to each other in the east of 113.95° E. The POC concentration in region B was less affected by freshwater than that in region A, and did not change significantly from 2002 to 2014 (Figure 7).

Influenced by the East Asia Monsoon, discharge from the Pearl River differs greatly with season. About 80% of freshwater is discharged into the PRE during the wet season (April–September), and only 20% occurs during the dry season [17]. While freshwater brings terrestrial POC into the PRE [12,15], the additional transported nutrients can also trigger algal growth [35]. Under the influences of freshwater, seasonal POC concentrations from 2002 to 2014 along the section (Figure 5) in summer, with higher discharge, were generally greater than those in other seasons (Figures 5 and 6). However, high turbidity in near-shore waters can also prevent phytoplankton from growing due to light limitation [16,43]. This might be the reason why POC concentrations in near-shore waters were lower in summer than those in autumn and winter (Figure 6). Furthermore, discharge in summer might also differ greatly with days. For example, discharge from the Pearl River on 6 July, measured at Gaoyao, Shijiao, and Boluo hydrometric stations (http://xxfb.hydroinfo.gov.cn), was greater than that on 31 July [17]. Similarly, POC concentrations in the northern PRE on 6 July 2011, were apparently greater than those on 31 July 2011 (Figure 11). Temporal distribution of POC differed greatly with discharge changing in an identical season, with higher POC concentration observed following greater discharge.

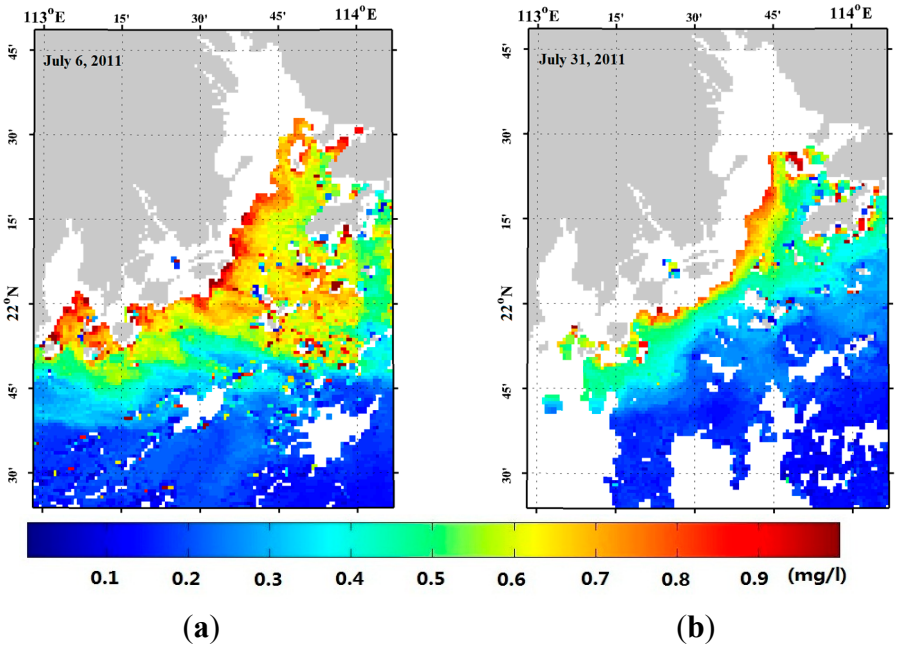

Figure 11. Satellite-derived POC concentrations in summer with different discharge from the Pearl River on (**a**) 6 July 2011; (**b**) 31 July 2011. Valid POC concentrations in the white regions were not obtained due to cloud cover, contamination by sun-glint, band saturation of MODIS, *etc.*

During the wet season, the plume of the Pearl River flows eastward and offshore under the impact of southwest wind [17,44]. Therefore, POC concentrations south of Hong Kong in summer were greater than those in other seasons (Figure 5). However, the plume is advected westward due to northeast wind during the dry season, so the eastward expansion of high POC concentrations is much smaller in winter and spring [17,44]. The high POC concentrations around the Wanshan Archipelago might be due to high phytoplankton production in low velocity water or POC discharged from surrounding islands. Other factors that influence phytoplankton growth might also have influenced POC distribution in the PRE, including coastal upwelling [45] and air temperature [1,2,6].

7. Conclusions

Under the influence of the East Asian Monsoon, most freshwater from the Pearl River occurs during the wet season. The POC (%TSM) in a monsoon river differs greatly to that in non-monsoon river. In this paper, an algorithm was developed to estimate surface POC concentrations in the PRE using remote sensing reflectance ratios. The algorithm was applied to MODIS/AQUA data to monitor POC concentration in the PRE dynamically. Importantly, it could describe high POC concentrations (>0.8 mg/L) in near-shore waters.

In the PRE, phytoplankton contribution to POC differed in different waters and changed with the seasons. Phytoplankton contributed more to POC in in-shore waters than that in off-shore waters in winter, but showed the inverse pattern in autumn and spring. Water masses mixing influenced the distribution of POC in the PRE. The temporal distribution of POC in the PRE was negatively affected by discharge from the Pearl River. Even with more POC from the Pearl River, POC concentration was lower at high flow on account of light limitation to phytoplankton growth. Moreover, POC concentrations in off-shore waters did not change significantly in the past decade; but POC concentrations in in-shore waters fluctuated with discharge from the Pearl River. Considering spatial characteristics, decreasing seasonal POC along a specific vertical to water depth gradient section could be fitted by exponential function ($y = ae^{bx}$, $b < 0$) in all seasons.

Rich nutrients brought by river might result in phytoplankton flourish and increase POC concentration in estuary. Terrestrial and aquatic POCs in estuary experience a series of complicated physical and biogeochemical reactions before being transported far away. Reflectance ratios of the developed algorithm use common-used bands of ocean color sensors, such as geostationary ocean color imager (GOCI), medium-resolution imaging spectrometer (MERIS), visible infrared imaging radiometer suite (VIIRS), *etc.* Based on these global covering satellite data, we can monitor POC dynamic changes in highly turbid waters of worldwide estuaries using the developed algorithm. Furthermore, POC concentration calculated from satellite data and water flux estimated through numerical model simulation can be combined to compute the POC flux from coastal ocean to open sea. All in all, the developed algorithm can be applied to explore sources, distributions, and dynamic changes of POC in estuaries using ocean color satellite data. Based on this POC information, we can explore POC budgets in global estuaries and improve management policies.

Acknowledgments

The authors would like to thank the Level 1 and Atmosphere Archive and Distribution System for providing MODIS product datasets. This study was supported by the National Basic Research Program ("973" Program) of China (grant 2015CB954002), the Public Science and Technology Research Fund Projects for Ocean Research (grant 201505003), the National Natural Science Foundation of China (grants 41476155, 41322039, and 41271378), and the "Global Change and Air-Sea Interaction" project of China (grant GASI-03-03-01-01).

Author Contributions

Delu Pan had the original idea. Dong Liu designed the algorithm and analyzed most data. Yan Bai help writing and revising the manuscript. Xianqiang He contributed with ideas and discussions. Difeng Wang contributed with preprocessing of remote sensing data. Ji-An Wei sampled and measured part of in-situ data. Lin Zhang measured part of in-situ data.

Conflicts of Interest

The authors declare no conflict of interest.

References

1. Zhu, Z.Y.; Zhang, J.; Wu, Y.; Lin, J. Bulk particulate organic carbon in the East China Sea: Tidal influence and bottom transport. *Prog. Oceanogr.* **2006**, *69*, 37–60.
2. Stramska, M. Particulate organic carbon in the global ocean derived from SeaWiFS ocean color. *Deep Sea Res. I* **2009**, *56*, 1459–1470.
3. Son, Y.B.; Gardner, W.D.; Mishonov, A.V.; Richardson, M.J. Multispectral remote-sensing algorithms for particulate organic carbon (POC): The Gulf of Mexico. *Remote Sens. Environ.* **2009**, *113*, 50–61.
4. Jahnke, R.A. The global ocean flux of particulate organic carbon: Areal distribution and magnitude. *Glob. Biogeochem. Cycles* **1996**, *10*, 71–88.
5. Stramska, M.; Stramski, D. Variability of particulate organic carbon concentration in the north polar Atlantic based on ocean color observations with SeaWiFS. *J. Geophys. Res.* **2005**, *110*, doi:10.1029/2004jc002762.
6. Gardner, W.D.; Mishonov, A.V.; Richardson, M.J. Global POC concentrations from *in situ* and satellite data. *Deep Sea Res. II* **2006**, *53*, 718–740.
7. Stramski, D.; Reynolds, R.A.; Babin, M.; Kaczmarek, S.; Lewis, M.R.; Röttgers, R.; Sciandra, A.; Stramska, M.; Twardowski, M.S.; Franz, B.A.; *et al.* Relationships between the surface concentration of particulate organic carbon and optical properties in the eastern South Pacific and eastern Atlantic Oceans. *Biogeosciences* **2008**, *5*, 171–201.
8. Mishonov, A.V.; Gardner, W.D.; Richardson, M.J. Remote sensing and surface POC concentration in the South Atlantic. *Deep Sea Res. II* **2003**, *50*, 2997–3015.
9. Stramski, D.; Reynolds, R.A.; Kahru, M.; Mitchell, B.G. Estimation of particulate organic carbon in the Ocean from satellite remote sensing. *Science* **1999**, *285*, 239–241.

10. Duforêt-Gaurier, L.; Loisel, H.; Dessailly, D.; Nordkvist, K.; Alvain, S. Estimates of particulate organic carbon over the euphotic depth from *in situ* measurements. Application to satellite data over the global ocean. *Deep Sea Res. I* **2010**, *57*, 351–367.
11. Wang, G.; Zhou, W.; Gao, W.; Yin, J.; Yang, Y.; Sun, Z.; Zhang, Y.; Zhao, J. Variation of particulate organic carbon and its relationship with bio-optical properties during a phytoplankton bloom in the Pearl River estuary. *Mar. Pollut. Bull.* **2011**, *62*, 1939–1947.
12. Liu, Q.; Huang, X.; Zhang, X.; Zhang, L.; Ye, F. Distribution and sources of particulate organic carbon in the Pearl River Estuary in summer 2010. *Acta Ecol. Sin.* **2012**, *32*, 4403–4412. (In Chinese)
13. Wang, X.; Ma, H.; Li, R.; Song, Z.; Wu, J. Seasonal fluxes and source variation of organic carbon transported by two major Chinese Rivers: The Yellow River and Changjiang (Yangtze) River. *Glob. Biogeochem. Cycles* **2012**, *26*, doi:10.1029/2011GB004130.
14. Zhu, C.; Wagner, T.; Pan, J.; Pancost, R. Multiple sources and extensive degradation of terrestrial sedimentary organic matter across an energetic, wide continental shelf. *Geochem. Geophys. Geosyst.* **2011**, *12*, doi:10.1029/2011GC003506.
15. Ni, H.; Lu, F.; Luo, X.; Tian, H.Y.; Zeng, E.Y. Riverine inputs of total organic carbon and suspended particulate matter from the Pearl River Delta to the coastal ocean off South China. *Mar. Pollut. Bull.* **2008**, *56*, 1150–1157.
16. Chen, Z.; Li, Y.; Pan, J. Distributions of colored dissolved organic matter and dissolved organic carbon in the Pearl River Estuary, China. *Cont. Shelf Res.* **2004**, *24*, 1845–1856.
17. Bai, Y.; Huang, T.; He, X.; Wang, S.; Hsin, Y.; Wu, C.; Zhai, W.; Lui, H.; Chen, C.A. Intrusion of the Pearl River plume into the main channel of the Taiwan Strait in summer. *J. Sea Res.* **2015**, *95*, 1–15.
18. Cai, W.; Guo, X.; Chen, C.A.; Dai, M.; Zhang, L.; Zhai, W.; Lohrenz, S.E.; Yin, K.; Harrison, P.J.; Wang, Y. A comparative overview of weathering intensity and HCO_3^- flux in the world's major rivers with emphasis on the Changjiang, Huanghe, Zhujiang (Pearl) and Mississippi Rivers. *Cont. Shelf Res.* **2008**, *28*, 1538–1549.
19. Knap, A.H.; Michaels, A.; Close, A.R.; Ducklow, H.; Dickson, A.G. *Protocols for the Joint Global Ocean Flux Study (JGOFS) Core Measurements*; IOC Manuals and Guides No. 29; United National Educational, Scientific and Cultural Organization (UNESCO): Paris, France, 1994.
20. Liu, Q.; Pan, D.; Bai, Y.; Wu, K.; Chen, C.A.; Liu, Z. Estimating dissolved organic carbon inventories in the East China Sea using remote-sensing data. *J. Geophys. Res. Oceans* **2014**, *119*, 6557–6574.
21. He, X.; Bai, Y.; Pan, D.; Huang, N.; Dong, X.; Chen, J.; Chen, C.A.; Cui, Q. Using geostationary satellite ocean color data to map the diurnal dynamics of suspended particulate matter in coastal waters. *Remote Sens. Environ.* **2013**, *113*, 225–239.
22. Mueller, J.L.; Fargion, G.S.; McClain, C.R. Ocean optics protocols for satellite ocean color sensor. In *Special Topics in Ocean Optics Protocols and Appendices*; Goddard Space Flight Center: Greenbelt, MD, USA, 2003.
23. Wang, M.; Shi, W. The NIR-SWIR combined atmospheric correction approach for MODIS ocean color data processing. *Opt. Express* **2007**, *15*, 15722–15733.
24. Bai, Y.; Pan, D.; Cai, W.; He, X.; Wang, D.; Tao, B.; Zhu, Q. Remote sensing of salinity from satellite-derived CDOM in the Changjiang River dominated East China Sea. *J. Geophys. Res. Oceans* **2013**, *118*, 227–243.

25. Świrgoń, M.; Stramska, M. Comparison of *in situ* and satellite ocean color determinations of particulate organic carbon concentration in the global ocean. *Oceanologia* **2015**, *57*, 25–31.
26. Le, C.; Li, Y.; Zha, Y.; Sun, D.; Huang, C.; Lu, H. A four-band semi-analytical model for estimating chlorophyll a in highly turbid lakes: The case of Taihu Lake, China. *Remote Sens. Environ.* **2009**, *113*, 1175–1182.
27. Dall'Olmo, G.; Gitelson, A.A. Effect of bio-optical parameter variability on the remote estimation of chlorophyll-a concentration in turbid productive water: Experimental results. *Appl. Opt.* **2005**, *44*, 412–422.
28. Wu, Y.; Zhang, J.; Liu, S.M.; Zhang, Z.F.; Yao, Q.Z.; Hong, G.H.; Cooper, L. Sources and distribution of carbon within the Yangtze River system. *Estuar. Coast. Shelf Sci.* **2007**, *71*, 13–25.
29. Wang, M.; Zhang, L.; Cui, Z. Spatial and temporal transport of organic carbon in Changjiang Mainstream and influence of Three Gorges Project. *Period. Ocean Univ. China* **2011**, *41*, 117–124. (In Chinese)
30. Meybeck, M. Carbon, nitrogen and phosphorus transport by world rivers. *Am. J. Sci.* **1982**, *282*, 401–450.
31. Ittekkot, V. Global trends in the nature of organic matter in river suspensions. *Nature* **1988**, *332*, 436–438.
32. Zhang, L.; Zhang, X.; Wang, X.; Liu, F. Spatial and temporal distribution of particulate and dissolved organic carbon in Yellow River estuary. *Adv. Water Sci.* **2007**, *18*, 674–682. (In Chinese)
33. Ran, L.; Lu, X.X.; Sun, H.; Han, H.; Han, J.; Li, R.; Zhang, J. Spatial and seasonal variability of organic carbon transport in the Yellow River, China. *J. Hydrol.* **2013**, *498*, 76–88.
34. Coynel, A.; Seyler, P.; Etcheber, H.; Meybeck, M.; Orange, D. Spatial and seasonal dynamics of total suspended sediment and organic carbon species in the Congo River. *Glob. Biogeochem. Cycles* **2005**, *19*, doi:10.1029/2004GB002335.
35. Dagg, M.; Benner, R.; Lohrenz, S.; Lawrence, D. Transformation of dissolved and particulate materials on continental shelves influenced by large rivers: Plume processes. *Cont. Shelf Res.* **2004**, *24*, 833–858.
36. Hedges, J.I.; Clark, W.A.; Quay, P.D.; Richey, J.E.; Devol, A.H.; de M. Santos, U. Compositions and fluxes of particulate Organic material in the Amazon River. *Limnol. Oceanogr.* **1986**, *31*, 717–738.
37. Zhang, L.; Qin, X.; Yang, H.; Huang, Q.B.; Liu, P.Y. Transported fluxes of the riverine carbon and seasonal variation in Pearl River basin. *Environ. Sci.* **2013**, *34*, 3025–3034. (In Chinese)
38. Kaiser, D.; Unger, D.; Qiu, G. Particulate organic matter dynamics in coastal systems of the northern Beibu Gulf. *Cont. Shelf Res.* **2014**, *82*, 99–118.
39. Eppley, R.W. Standing stocks of particulate carbon and nitrogen in the equatorial Pacific at 150 W. *J. Geophys. Res.* **1992**, *97*, 655–661.
40. He, B.; Dai, M.; Zhai, W.; Wang, Z.; Wang, K.; Chen, J.; Lin, J.; Xu, Y. Distribution, degradation and dynamics of dissolved organic carbon and its major compound classes in the Pearl River estuary, China. *Mar. Chem.* **2010**, *119*, 52–64.
41. Bauer, J.E.; Cai, W.; Raymond, P.A.; Bianchi, T.S.; Hopkinson, C.S.; Regnier, P.A.G. The changing carbon cycle of the coastal ocean. *Nature* **2013**, *504*, 61–70.

42. Cauwet, G.; Miller, A.; Brasse, S.; Fengler, G.; Mantoura, R.F.C.; Spitzy, A. Dissolved and particulate organic carbon in the western Mediterranean Sea. *Deep Sea Res. II* **1997**, *44*, 769–779.
43. Pennock, J.R.; Sharp, J.H. Temporal alternation between light- and nutrient-limitation of phytoplankton production in a coastal plain estuary. *Mar. Ecol. Prog. Ser.* **1994**, *111*, 275–288.
44. Dong, L.; Su, J.; Wong, L.A.; Cao, Z.; Chen, J.C. Seasonal variation and dynamics of the Pearl River plume. *Cont. Shelf Res.* **2004**, *24*, 1761–1777.
45. Roegner, G.C.; Shanks, A.L. Import of coastally-derived Chlorophyll a South Slough, Oregon. *Estuaries* **2001**, *24*, 244–256.